Pergamon
PII: S0022-4073(96)00043-X
J. Quant. Spectrosc. Radiat. Transfer Vol. 56, No. 2, pp. 209–224, 1996

0022-4073/96 $15.00 + 0.00

DOAS FOR FLUE GAS MONITORING—II. DEVIATIONS FROM THE BEER–LAMBERT LAW FOR THE U.V./VISIBLE ABSORPTION SPECTRA OF NO, NO_2, SO_2 AND NH_3

JOHAN MELLQVIST[a,b] and ARNE ROSÉN[a]

[a]Department of Physics, Chalmers University of Technology and Göteborg University, S-412 96 Göteborg and [b]The Swedish Environmental Research Institute (IVL) P.O. Box 47086, S-402 58 Göteborg, Sweden

(Received 14 December 1995)

Abstract—Deviations from the Beer–Lambert law were studied for the differential absorption cross-sections for NO, SO_2, NO_2 and NH_3. This was performed by simple calculations, computer simulations of spectra and by recordings of spectra for the above mentioned species at various total columns. The linearity studies for the DOAS instrument displayed large variations for the molecules studied and for different wavelength bands. In a calculation it was shown that the optical depth deviated from a linear concentration dependence by a term which was directly proportional to the statistical variance of the true absorption cross sections and proportional to the square of the total column, under the assumption of a boxcar instrument lineshape. Species exhibiting little variance or fine structure in their spectra, for instance NO_2, displayed a larger linear region compared with molecules exhibiting a rich structure, i.e., NO. The former species was linear to a total column of 3150 mg/m^2, which correspond to a maximum optical depth of 0.7, while the latter was linear to only 6 mg/m^2, corresponding to a maximum optical depth of 0.024, in the resolution range studied. The linear regions for the other species studied were 90 mg/m^2 for SO_2 at 230 nm, 180 mg/m^2 for SO_2 at 300 nm and 36 mg/m^2 for NH_3. The main effect of the nonlinearity was to cause a reduction in the peak height of the absorption. It was shown that the nonlinearity effect is independent on the spectral resolution when a large number of absorption lines are covered by the bandpass of the instrument. It was also shown that the largest change in linearity occurs when the resolution is similar in magnitude to the absorption linewidth. The nonlinear behavior for NO varied less than 2% in the temperature range 300–1000 K and the spectral resolution range 0.25–1 nm. The nonlinearity effect caused quantitative rather than qualitative changes of the spectral features and typical relative errors can be as high as 35% in a flue gas. Copyright © 1996 Elsevier Science Ltd

1. INTRODUCTION

Differential Optical Absorption Spectroscopy (DOAS) is today used in a broad number of applications, for example long-term measurements of concentrations of trace species in the stratosphere[1,2] and environmental monitoring of main pollutants in urban areas.[5] The technique is based on the recording of differential absorption, i.e., the difference between local maxima and minima in the u.v./visible absorption spectrum of the probed gas species.

One application that is focused on in this paper, but also in several previous papers,[6–8] is the use of DOAS for in-situ measurements of hot flue gases, by transmitting u.v.-light directly across a flue gas channel. In order to perform accurate DOAS measurements there are two main aspects that have to be considered, compared with using DOAS for atmospheric applications, and that is so called *temperature* and *nonlinearity effects*. The temperature effects have been studied in a separate publication[9] which we from now on will denote as Paper I, and they are caused by the fact that the magnitude of the differential absorption cross sections used by the DOAS technique change with temperature.

The nonlinearity effects on the other hand are caused by the fact that the molecular absorptions can deviate from the Beer–Lambert law at large optical depths.[10,11] When probing across a flue gas

channel, the optical pathlength is more or less determined by the dimensions of the flue gas channel. Since the concentration of several polluters can be rather high in flue gases the absorption of gas species in flue gases can easily deviate from the Beer–Lambert law and become nonlinear.

The existence of nonlinearity effects has long been known in absorption spectroscopy[10,11] and commercial instruments utilizing molecular absorption actually corrects for such nonlinearities. Most studies have been performed experimentally for measurements of single lines in the infrared region, however. In this study we have studied nonlinearity effects in the u.v./visible when using a medium resolution grating spectrometer at resolutions between 0.3 and 1 nm and at atmospheric pressure and temperature. Under these conditions large number of rovibronic absorption lines are covered by the bandpass of the spectrometer, and the measurement situation is therefore more complicated than when recording a single line. In addition we are concerned with nonlinearity effects obtained when using DOAS and this complicates things even further, since the differential absorption (difference in absorption between different wavelengths) and not the absolute absorption is being used in the DOAS technique. To our knowledge this has not been studied in particular. The linearities for NO, NO_2, SO_2 and NH_3 have therefore been studied in this work for the DOAS technique by experimental recordings, by computer simulations and by a few simple, but quite instructive, calculations.

2. EXPERIMENTAL

A grating spectrometer (Thermo Jarrel Ash, Czerny–Turner, 275 mm, f/3.8) with a resolution between 0.2 and 0.5 nm was used to record absorption spectra of various species. The recordings were performed in two different Pyrex™-glass cells with optical path-lengths of 0.46 and 2 m, and diameters of 9 and 6 cm, respectively. A schematic drawing of the experimental equipment is shown in Fig. 1. Broad band u.v./visible light from a xenon-lamp is here transmitted through a measurement cell and then via a fiber further transmitted into a grating spectrometer. The spectra are scanned by the use of a *slotted disc* device and a photomultiplier tube. The spectra are stored and analyzed in a PC. The experimental equipment has been further described in Paper I[9] and the DOAS equipment is of the same design as that introduced by Platt and Perner.[12]

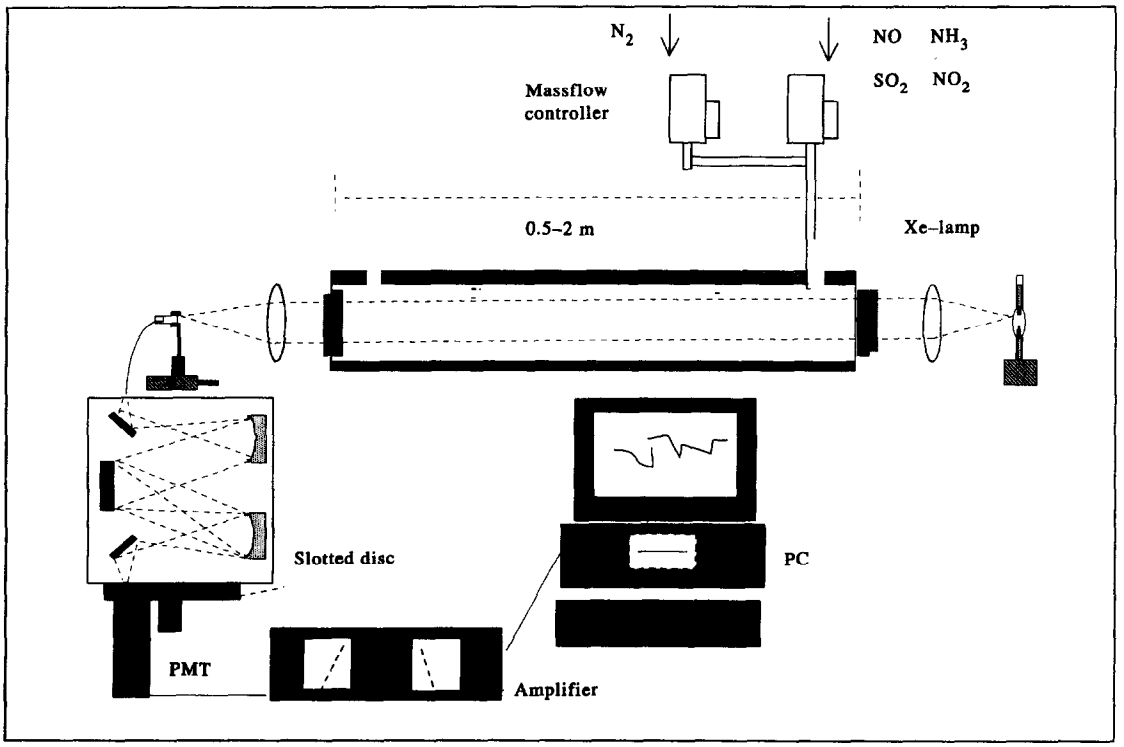

Fig. 1. The experimental setup for the nonlinearity measurements.

The gases used were supplied from AGA specialgas AB in Sweden at specific volume concentrations, with a mixing precision of 5%. In order to achieve different total columns in the measurement cell the gases were blended with pure nitrogen using massflow controllers (Brooks, The Netherlands) with a mixing precision of 1%. The spectral recordings were performed at room temperature (293 K) and atmospheric pressure. For several of the species studied, optical filters were used to reduce the photodissociation and stray light in the spectrometer, this was also described in Paper I.[9] The measurements were performed at rather high flow rates, between 2 and 7 l/min, in order to suppress wall effects.

3. THEORY

Two centuries ago it was discovered by J. H. Lambert that the light intensity decreases exponentially as a function of traveled distance in an absorbing medium. Later A.v Beer discovered that the absorption is proportional to the logarithm of the concentration of the absorbing medium. These two discoveries constitute the Beer–Lambert law which is fundamental in absorption spectroscopy. It can be derived from the assumption that the amount of intensity, dI, which is absorbed when light with initial intensity I_0 is transmitted a distance dx in an absorbing medium, with absorption cross section σ and concentration c, is proportional to: $dI = \sigma \cdot c \cdot I \cdot dx$. Solving the differential equation yields:

$$I_{\text{det}}(\lambda, T, p, \ldots) = I_0(\lambda) \cdot \exp[-\sigma(\lambda, T, p, \ldots) \cdot c \cdot x] \tag{1}$$

where

$I_{\text{det}}(\lambda)$ = detected light intensity
σ = absorption cross section (cm^2/molecule)
c = number density of absorbing molecule (molecules/cm^3)
I_0 = background intensity
x = optical pathlength (cm).

The Beer–Lambert law in Eq. (1) is applied in measurement instruments based on light absorption. In a strict sense the equation is only valid for instruments with an infinite resolution, however. Since this is not the case, the true absorption is not recorded but rather the average absorption over the bandpass of the instrument. The absorption will therefore not always obey the Beer–Lambert law, and in this case one says it has become *nonlinear*.

From the terms given in Eq. (1) the *optical depth* (OD) can be defined as $(\sigma \cdot c \cdot x)$ and the *total column* as $(c \cdot x)$, and these will be frequently used hereafter.

3.1. Retrieval algorithms

In the spectral evaluation routines of the DOAS technique a polynomial, I_p, of low order (1st–5th) is fitted through the recorded spectrum. The original spectrum is then divided with the polynomial and the logarithm of this ratio corresponds to the differential absorbance spectrum, which is proportional to the concentration of the measured molecule according to the following expression:

$$\ln\left(\frac{I_{\text{det}}(\lambda)}{I_p(\lambda)}\right) = d\sigma(\lambda) \cdot c \cdot x = dA \tag{2}$$

where dA corresponds to the differential absorbance and $d\sigma$ to the differential absorption cross section. Equation (2) is the basis for the spectral evaluation algorithms in the DOAS technique and can be derived from the Beer–Lambert law, which was done in Paper I.[9] The polynomial eliminates the influence of scattering from particles and molecules and other broad wavelength dependencies in the spectrum. It also removes the broad absorption features of the molecule and will thus decrease the effective absorption cross section yielding a pseudo absorption cross section which is named *differential absorption cross section*. Since the polynomial is of low order it is assumed that it does not affect the appearance and magnitude of the narrow spectral structure which is utilized for the evaluation of the concentration. This is entirely correct only at small optical depths, however, since the narrow absorption features becomes broader with increasing optical depth,

as was discussed in Paper I.[9] Also for larger ODs it is usually possible to use Eq. (2), since the polynomials are of such low order so that even if the narrow absorption features of the molecule have broadened they are still much narrower than the polynomial. For several molecules it is possible to fit a spline through fixed wavelengths points in the intensity spectrum. The differential absorption cross-sections will then be defined as the difference between the true absorption cross-sections and the spline.

The fitting procedure was performed by multiple linear regression in accordance with Bevington.[13] The laboratory spectra were here fitted linearly to the experimental spectra, and a scaling factor and a baseline was obtained, yielding the smallest difference between the two spectra. The correlation coefficient and standard deviation between the fitted and experimental spectra were also calculated in the fitting procedure and these parameters were good indicators of the quality of the fit and the measurements.

The retrieval algorithms of the recorded DOAS spectra in this study were consistent with the procedures of Platt and Perner[12] and can be summarized with the following operations which were performed on the recorded intensity spectra: (i) background subtraction, (ii) normalization with a lamp- or clean air reference, (iii) normalization with a fitted polynomial (1st–5th order) or spline, (iv) logarithmic transformation, (v) spectral fitting to calibration spectra.

3.2. Spectral evaluation regions

In Figs. 2 and 3 below, spectral features of the species studied are shown in the regions in which the DOAS evaluation is performed. In Fig. 2 the absorption cross sections for SO_2 around 300 nm are displayed and these were recorded by Carleer.[14] The absorption features of this species correspond to a narrow sinusoidal structure, superimposed on a rather smooth background. When deriving the differential absorbance spectra according to Eq. (2) the smooth absorption structure will be removed, thus leaving only the narrow structure to be used in the DOAS evaluation.

In Fig. 3 the absorption features of NH_3, NO_2, NO and SO_2 are shown, in the spectral regions that were used in this study. It can be seen that the absorption features of NO_2 are similar to the ones of SO_2, with narrow structures superimposed on a smooth background. For the absorption features of both NH_3 and SO_2 around 226 nm, the smooth background structure is rather small compared to the narrow absorption features. The absorption features of NO on the other hand contain no smooth background and for this species the total rather than the differential absorption can be used for the measurements. In Table 1 are shown the evaluation regions and types of polynomial used, for the derivation of DOAS spectra from the initially recorded intensity spectra.

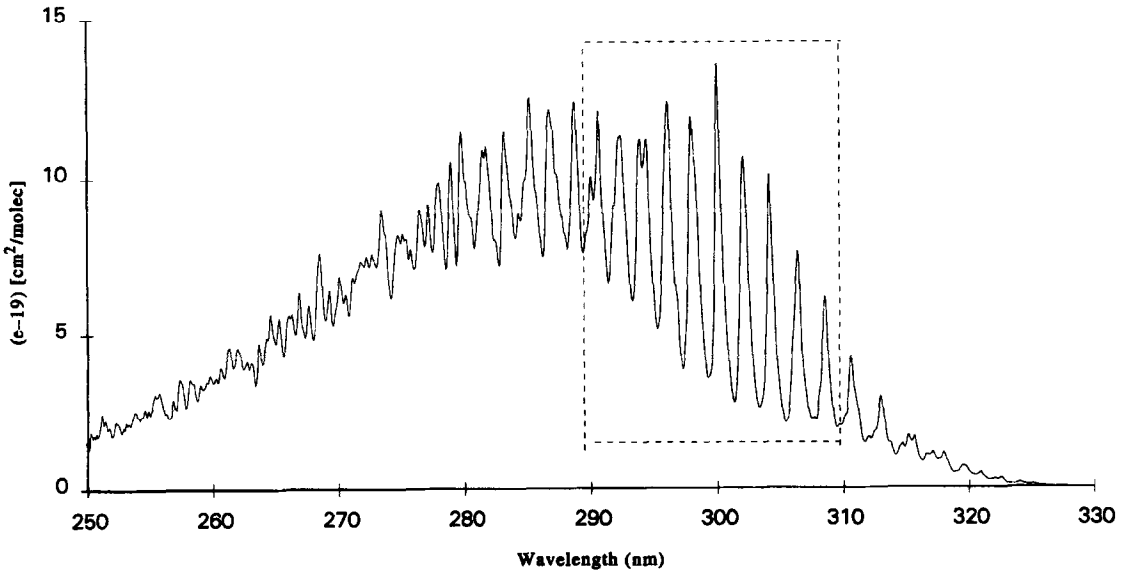

Fig. 2. Absorption cross sections of SO_2 by Carleer.[14] The region used for the SO_2 evaluation in this study is also shown within the dotted frame.

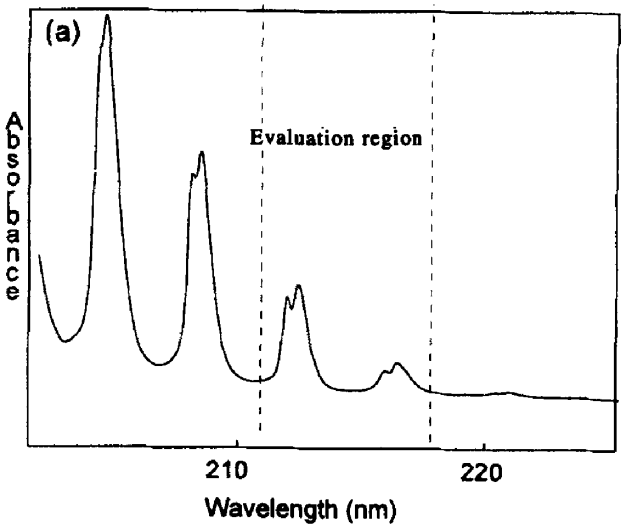

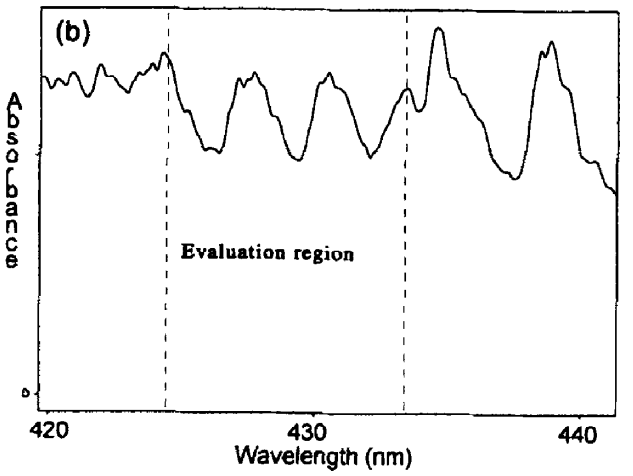

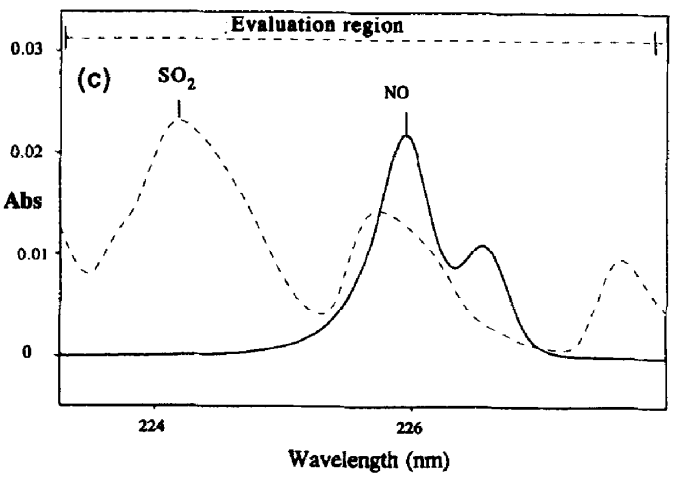

Fig. 3. Absorbance spectra and evaluation region (dotted) of NH_3 (a), NO_2 (b) and NO and SO_2 (c).

Table 1. Evaluation regions and type of polynomial for the derivation of differential optical absorption spectra.

Species	Evaluation region (nm)	Order of polynomial
NO	223–228	Spline†
SO_2	223–228	5th order
NH_3	214–217	4th order/spline
SO_2	295–305	5th order
NO_2	425–435	1st order spline

†All splines are of first order.

3.3. *Spectral simulations*

The spectral simulations of NO were performed for the $\gamma(0,0)$-band between 220 and 230 nm. This band corresponds to an electronic transition from the ground state $X^2\Pi$ to the upper level $A^2\Sigma$, coupled with superimposed vibrational and rotational transitions. The simulations were carried out at various column densities and temperatures using a PC-based computer code which was developed from algorithms by Wahnström.[15] Molecular parameters from Huber and Herzberg[16] were used to calculate energy levels and transition strengths. Neither the oscillator strength, nor the Franck–Condon factor were calculated. Instead the Hönl–London transition strengths were calculated as relative values using algorithms derived by Hill.[17] In order to obtain absolute absorption cross-sections the calculated spectra were compared with and scaled to experimental spectra. The calculated absorption cross-sections at various temperatures were converted to DOAS spectra at atmospheric pressure by adding Voigt broadening, with a pressure broadening coefficient of 0.56 cm^{-1}, to the calculated absorption cross-sections.[18] The absorption cross-sections were then convoluted with the *instrument line shape* (ILS) function for the DOAS instrument in use. Figure 4 gives a good overview over the performed spectral simulation. The simulated true atmospheric transmittance for a total column of 12.6 mg/m^2 of NO, is displayed as (A) together with the ILS function of the DOAS instrument (B) in this study. The result of the convolution between the two latter spectra is also displayed (C) and it corresponds to the apparent transmittance which is detected by the DOAS instrument. It can be seen that within the bandpass of the instrument a large number of absorption lines (10–30) are covered. The ILS function was obtained by recording the line profile of a low-pressure mercury lamp at 253.8 nm with the DOAS instrument. A more detailed explanation of the spectral simulations is given in Paper I.[9]

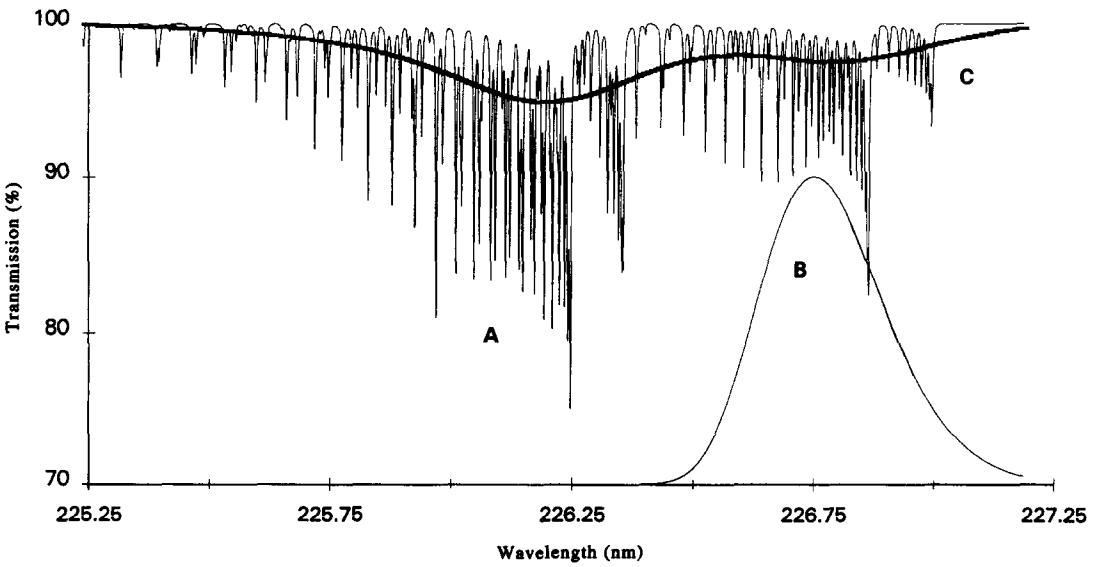

Fig. 4. (A) Simulated true transmission spectrum of NO calculated at a total column of 12.6 mg/m^2, 1 atm and 300 K; (B) ILS function of the DOAS instrument; (C) the resulting simulated DOAS spectrum, obtained from a convolution between A and C, i.e., $C = A \otimes B$.

4. RESULTS

4.1. Derivation of apparent optical depth

The light intensity that is recorded by the DOAS instrument at a certain wavelength, λ_0, corresponds to the through-the-air transmitted light intensity convoluted with the ILS function of the instrument:

$$I_{det}(\lambda_0) = I_0 \int_0^{\infty} \exp[-\sigma(\lambda)\cdot c\cdot x]\cdot \mathrm{ILS}(\lambda - \lambda_0)\cdot \mathrm{d}\lambda \tag{3}$$

where the variables are the same as defined in Eq. (1). If the ILS function is assumed to be rectangular (boxcar) with a value of unity, then the recorded intensity will simply correspond to the average transmittance over the bandpass, $\Delta\lambda$, of the spectrometer. The apparent optical depth (OD_{app}), which is obtained with the instrument at a certain wavelength, λ_0, can then be written in the following manner by the use of Eq. (3), the Beer–Lambert law and Taylor expansion of the exponential and logarithm functions:

$$\begin{aligned}
OD_{app}(\lambda_0) &= -\ln\left(\frac{I_{det}(\lambda_0)}{I_0(\lambda_0)}\right) = -\ln\left(\frac{\int_{\lambda_0-\Delta\lambda/2}^{\lambda_0+\Delta\lambda/2} \exp[-OD_{true}(\lambda)]\,\mathrm{d}\lambda}{\int_{\lambda_0-\Delta\lambda/2}^{\lambda_0+\Delta\lambda/2} 1\cdot \mathrm{d}\lambda}\right) \\
&= -\ln\left(\frac{\int_{\lambda_0-\Delta\lambda/2}^{\lambda_0+\Delta\lambda/2} \exp[-OD_{true}(\lambda)]\,\mathrm{d}\lambda}{\Delta\lambda}\right) \\
&= -\ln\left(1 - \frac{1}{\Delta\lambda}\int_{\lambda_0-\Delta\lambda/2}^{\lambda_0+\Delta\lambda/2} (OD_{true}(\lambda) - \tfrac{1}{2}OD_{true}^2 + O(3))\,\mathrm{d}\lambda\right) \\
&= \overline{OD}_{true} - \tfrac{1}{2}(\overline{OD_{true}^2} - \overline{OD_{true}}^2) + \tfrac{1}{6}(\overline{OD_{true}^3} + 2\overline{OD}_{true}^3 - 3\overline{OD_{true}}\cdot\overline{OD_{true}^2}) + O(4)
\end{aligned} \tag{4}$$

where I_0 corresponds to the average background intensity over the bandpass of the instrument, $O(4)$ corresponds to higher order terms, $\overline{OD}$ corresponds to the average of the optical depth and $\overline{OD^2}$ corresponds to the average of the square of the optical depth, and so forth for the other terms.

In order to facilitate the mathematical treatment, the terms in Eq. (4) can be written as sums instead of integrals, in the following way:

$$\overline{OD}_{true} = \frac{\int_{\lambda_0-\Delta\lambda/2}^{\lambda_0+\Delta\lambda/2} OD_{true}(\lambda)\,\mathrm{d}\lambda}{\Delta\lambda} \overset{N\to\infty}{=} \frac{1}{N}\sum_{i=1}^{N}[OD_i] = \frac{1}{N}cx\sum_{i=1}^{N}\sigma_i = cx\bar{\sigma}. \tag{5}$$

In the same manner one can write:

$$\overline{OD}_{true}^2 - \overline{OD_{true}^2} = \frac{1}{N}\sum_{i=1}^{N} OD_i^2 - \left(\frac{1}{N}\sum_{i=1}^{N} OD_i\right)^2 = (cx)^2\frac{1}{N}\left(\sum_{i=1}^{N}\sigma_i^2 - \frac{1}{N}\left(\sum_{i=1}^{N}\sigma_i\right)^2\right). \tag{6}$$

The last term in Eq. (6) can be identified as the variance, $s^2(\sigma)$, of the true absorption cross sections over the bandpass of the instrument,[19] according to:

$$s^2(\sigma) = \frac{1}{N-1}\sum_{i=1}^{N}(\sigma_i - \bar{\sigma})^2 = \frac{1}{N-1}\left(\sum_{i=1}^{N}\sigma_i^2 - \frac{1}{N}\left(\sum_{i=1}^{N}\sigma_i\right)^2\right) \overset{N\to\infty}{\approx} \frac{1}{N}\left(\sum_{i=1}^{N}\sigma_i^2 - \frac{1}{N}\left(\sum_{i=1}^{N}\sigma_i\right)^2\right). \tag{7}$$

Equations (4), (5), (6) and (7) yield the following result:

$$\boxed{OD_{app}(\lambda_0) = \overline{OD}_{true} - (cx)^2\frac{s^2(\sigma)}{2} + O(3) = cx\bar{\sigma} - (cx)^2\frac{s^2(\sigma)}{2} + O(3)}. \tag{8}$$

Equation (8) thus states that the apparent OD at a certain wavelength, λ_0, deviates from the average of the true OD by a term which is quadratically dependent on the total column and directly

proportional to the variance of the true absorption cross sections, calculated over the bandpass of the instrument. The apparent OD will thus increase linearly with the total column only if (a) the total column is very small so that second order terms can be neglected or (b) the statistical variance of the absorption cross sections is zero over the bandpass of the instrument, which corresponds to a constant absorption cross section. In addition one should consider that the variance is proportional to the square of the absorption cross sections, as seen in Eq. (7), and the variance will therefore be unproportionally largest at the absorption peaks.

4.2. Calculation of nonlinearity with a boxcar ILS-function

A simple simulation of hypothetical spectra is useful in order to get an understanding of Eq. (8) and on how the statistical variance of the spectra affect the nonlinearity. Five hypothetical absorption cross section spectra were therefore simulated with different linewidths and number of lines. These are shown in Fig. 5 and are labeled with A–D. The spectra were all normalized to have the same integrated absorption cross section over the bandpass of a fictitious instrument. Spectrum A has the largest statistical variance and then the statistical variances successively decreases from spectra B to D. The variables used in the simulation of the spectra in Fig. 5 and the calculated statistical variances of the cross sections are shown in Table 2. Equation (8) was then used to calculate the apparent OD as a function of the true OD for the spectra A–D and this is shown in Fig. 6. It can be seen that spectrum D behaves linearly at virtually all optical depths while the other spectra are linear only for a small range of optical depths.

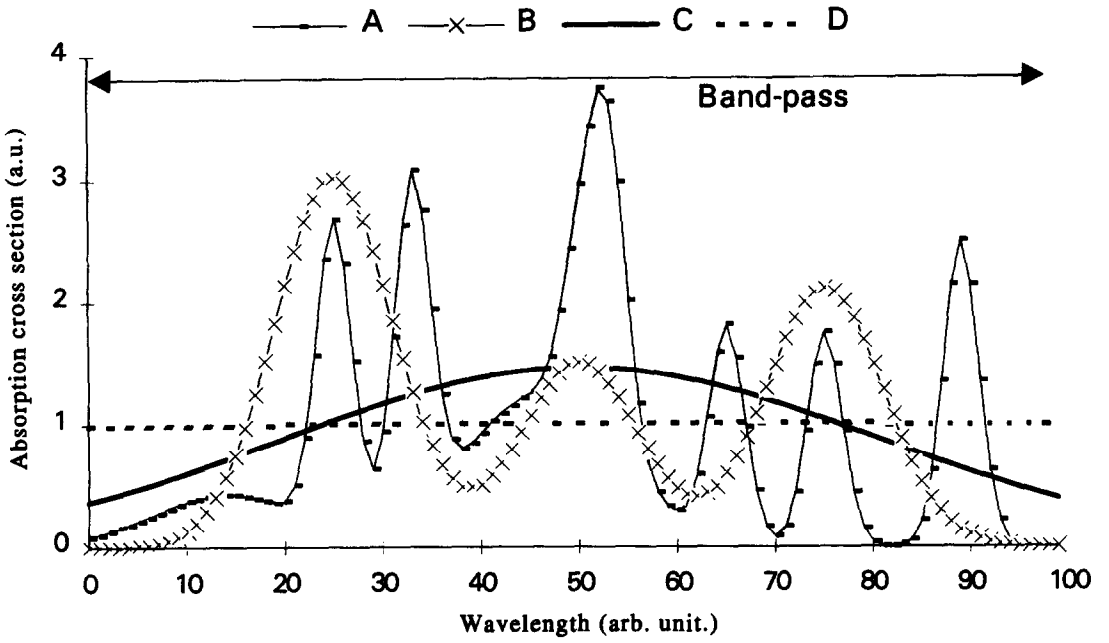

Fig. 5. Several hypothetical absorption cross sections displayed over the bandpass of an arbitrary instrument with a boxcar ILS-function (arbitrary units).

Table 2. Average of the absorption cross sections and variance calculated over a fictitious bandpass (width = 100) for the spectra shown in Fig. 5. The linear region was calculated by Eq. (8). All units are arbitrary.

Spectrum	Linewidth†	$\sigma_{average}$	$s^2(\sigma)$	Linear region‡ (OD)
A	3	1	0.88488	0.023
B	10	1	0.71755	0.028
C	50	1	0.12932	0.16
D	500	1	1.72E-05	1120

†FWHM of the single lines.
‡Less than 1% deviation from linearity.

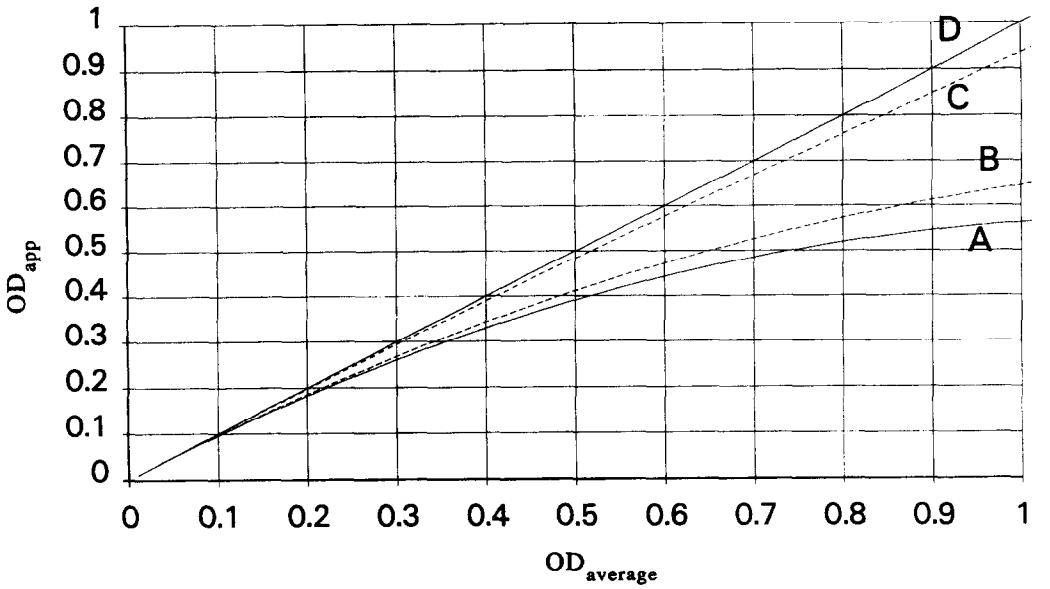

Fig. 6. Apparent OD of hypothetical species against true average OD.

The linear region is here defined as where the apparent OD deviates less than 1% from the true OD. The calculated linear regions for the spectra A–D in Fig. 5 are also given in Table 2.

Spectrum D in Fig. 5 corresponds to a Gaussian shaped absorption line with a width (FWHM) which is 5 times larger than the fictitious bandpass, and this example thus shows that a true absorption cross section will be obtained if the resolution is 5 times higher than the linewidth of the absorption line. This agrees well with the results of Andersson[11] in which it was found that a general rule of thumb when recording single absorption lines is that the bandpass of the instrument (FWHM) should be less than one-fifth of the absorption linewidth, in order to obtain a true value of the optical depth.

It should be noted that the region of linearity changes much more between spectra C and D than between spectra A and B, as seen in Table 2 and Fig. 6. This means that a change in instrumental resolution (bandpass) when the resolution is close to the linewidth will affect the region of linearity more than when changing the instrumental resolution in a situation where several absorption lines are recorded within the bandpass of the instrument. This can be intuitively understood from the variance term. If a species exhibits several identical absorption lines within the bandpass of an instrument, then the calculated variance will be independent on the number of absorption lines included in the calculation.

4.3. Calculation of nonlinearity with a Gaussian ILS-function

Equation (8) was developed under the assumption that third order terms in Eq. (6) could be neglected and that the ILS-function was of boxcar-type. For another type of ILS-function, e.g., Gaussian, Eq. (4) would still be valid, although all averages would have to be weighted with the ILS-function as given in Eq. (9). The intuitively simple expression in Eq. (8) would not be entirely valid however.

$$\mathrm{OD}_{\mathrm{app}}(\lambda_0) = c \cdot x \cdot \int_0^\infty \sigma_\lambda \cdot \mathrm{ILS}_{\lambda,\lambda_0} \cdot \mathrm{d}\lambda - \tfrac{1}{2} \cdot (c \cdot x)^2 \left(\int_0^\infty \sigma_\lambda \cdot \mathrm{ILS}^2_{\lambda,\lambda_0} \cdot \mathrm{d}\lambda - \left(\int_0^\infty \sigma_\lambda \cdot \mathrm{ILS}^2_{\lambda,\lambda_0} \cdot \mathrm{d}\lambda \right)^2 \right) + (O3). \tag{9}$$

Equation (9) was used to study how the apparent OD at the peak of a single Gaussian shaped absorption line was affected by the width of a Gaussian ILS-function. The Gaussian shaped absorption line was assumed to have a linewidth of Δ and a maximum cross section of σ_0. In addition the ILS-function was assumed to have a Gaussian shape, with a varying width of $(\xi \cdot \Delta)$.

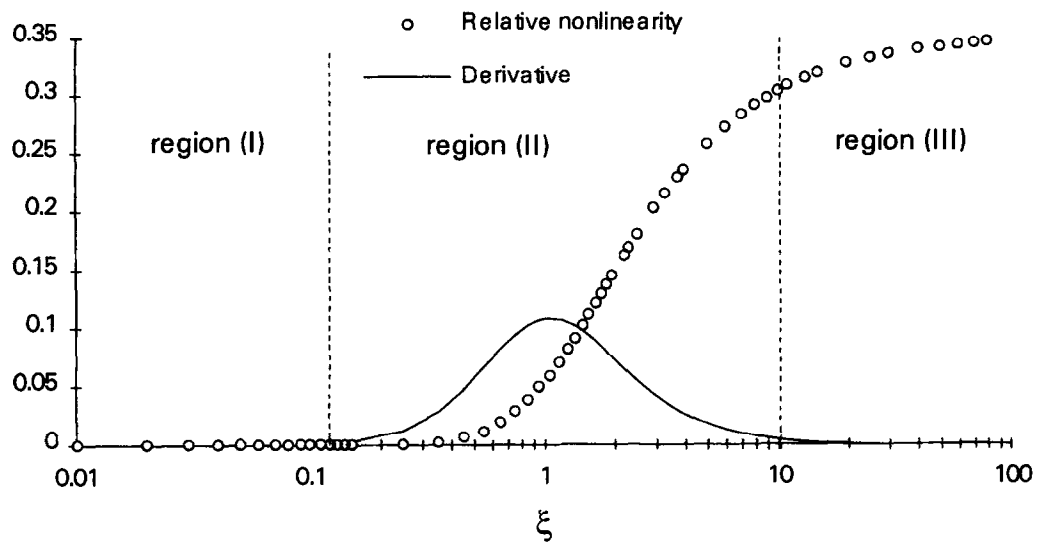

Fig. 7. The graph shows relative nonlinearity (A_2/A_1) and its derivative for a single Gaussian absorption line (FWHM = Δ) vs the relative width, ξ, of the ILS function (FWHM = $\xi \cdot \Delta$).

Equation (9) could then be rewritten as:

$$\mathrm{OD}_{\mathrm{app}}(\lambda_0) = A_1(\xi)\cdot(\sigma_0 \cdot c \cdot x) - A_2(\xi)\cdot(\sigma_0 \cdot c \cdot x)^2 + (O3) \tag{10}$$

where

$$A_1(\xi) = \left(\sqrt{\frac{1}{\xi^2+1}}\right), \quad A_2(\xi) = \frac{1}{2}\left(\sqrt{\frac{1}{2\xi^2+1}} - \frac{1}{\xi^2+1}\right). \tag{11}$$

We then define the *relative nonlinearity* as the ratio between the nonlinear and linear term in Eq. (10), i.e., (A_2/A_1).

In Fig. 7 the relative nonlinearity and its derivative are plotted as a function of the relative width, ξ, of the ILS-function, and three different regions can be identified. In region (I) the ILS-function is considerably narrower than the absorption line and the derivative indicates that the relative nonlinearity is almost constant as a function of the relative width of the ILS-function. In region (II) the relative nonlinearity has a considerably larger dependence on the relative width than in region (I) with a maximum in the derivative at a relative width of ($1.089 \cdot \mathrm{FWHM}_{\mathrm{abs.-line}}$). This means that when the spectral resolution of an absorption instrument is similar in magnitude to the absorption linewidth, the nonlinearity effect, for a single line, will change considerably with the resolution. In region (III) the relative nonlinearity again, as in region (I), becomes fairly constant and independent of the resolution. The relative nonlinearity reaches a maximum value of 0.35355. If the true optical depth at the absorption peak corresponds to unity ($\sigma_0 \cdot c \cdot x = 1$), a relative error of 35% will thus be obtained for the resulting apparent optical depth.

4.4. Simulation of nonlinearity in the absorption spectra of NO

So far only hypothetical examples of artificial spectra have been considered, which means that the conclusions drawn are valid for all types of absorption spectroscopy. We now consider the u.v. spectrum of NO around 226 nm. The true absorption of NO at atmospheric pressure and 300 K was shown in Fig. 4, obtained from a simulation of the absorption cross sections. The statistical variance and average of these absorption cross sections were calculated at the Q-branch over a spectral interval which corresponds to the FWHM bandpass of the spectrometer used in this study (226.1–226.4 nm). The variance and average terms were then put into Eq. (8), in order to calculate the apparent OD as a function of total column. This is shown in Fig. 8 together with a computer simulation for which the apparent OD was obtained from simulated spectra of NO, calculated for various total columns according to the description in Sec. 3.3. There is a good agreement between the calculated and computer simulated linearity curves up to a total column of 100 mg/m^2, thus indicating that Eq. (8) represents the nonlinearity effect well at small total columns.

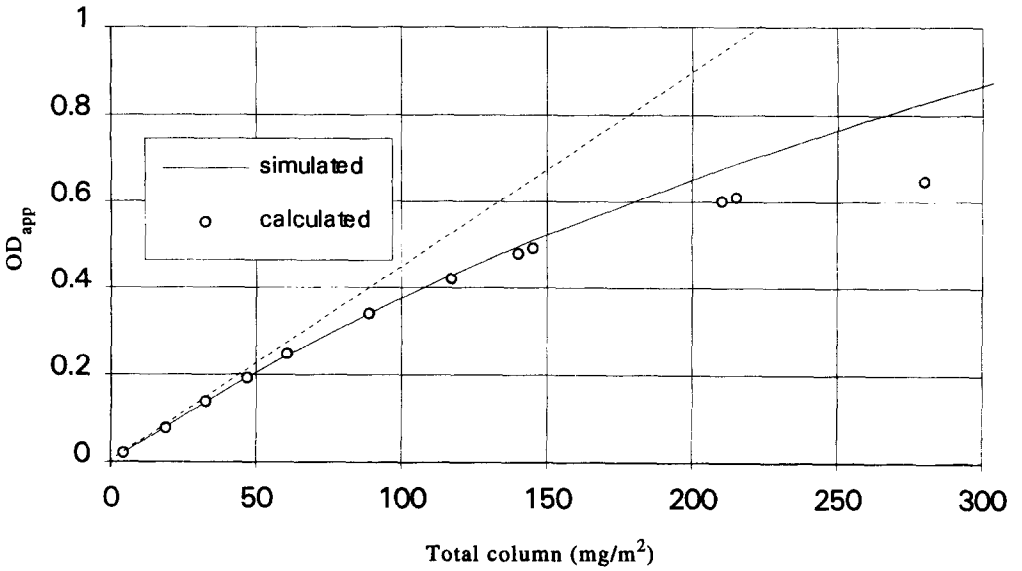

Fig. 8. Comparison of a linearity curve obtained from computer simulated NO spectra (simulated) and a linearity curve calculated by the use of Eq. (8) and the cross sections displayed in Fig. 4 (calculated).

Different ILS-functions were assumed for the simulated and calculated linearity curves in Fig. 8, however. A boxcar ILS function was assumed for the calculated linearity curve and a Gaussian ILS function for the simulated one. Despite this difference there is a good agreement between the two curves, and this may be explained by the fact that the linearity of NO is fairly independent of the spectral resolution of the instrument. This will be shown later in this section and can also be understood from the fact that a large number of absorption lines for NO are covered by the bandpass of the instrument, thus making the nonlinearity effect independent of spectral resolution, as was shown in Sec. 4.2.

The simulated NO spectra which were used to check the nonlinearity in Fig. 8 are now studied in more detail in order to describe how typical DOAS spectra are affected by the nonlinearity effect. Two simulated DOAS spectra of NO and their residual are displayed in Fig. 9. The spectrum with

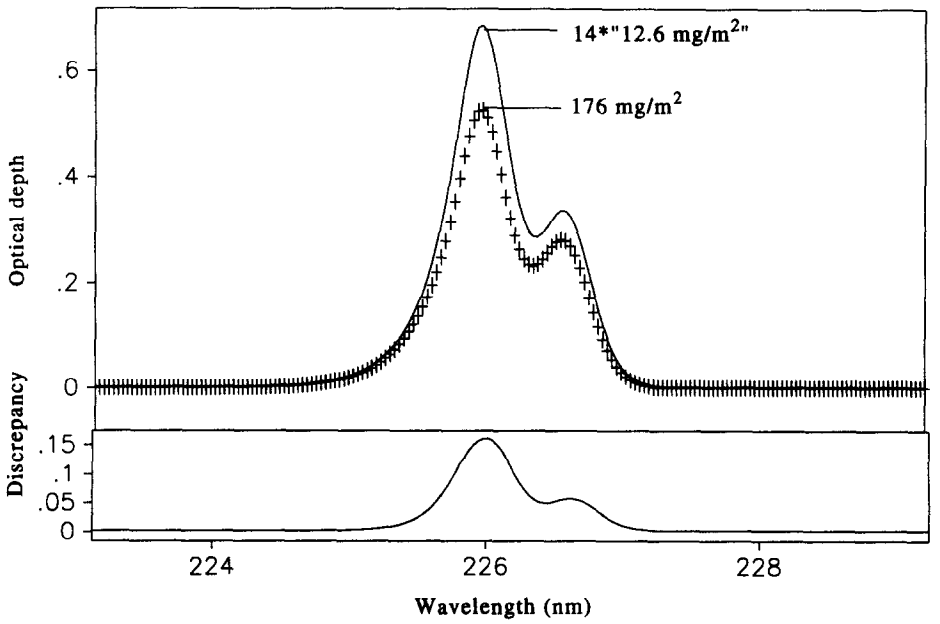

Fig. 9. Simulated spectra of NO for total columns of 12.6 and 176 mg/m^2, normalized to the same total column, and the residual between the two spectra.

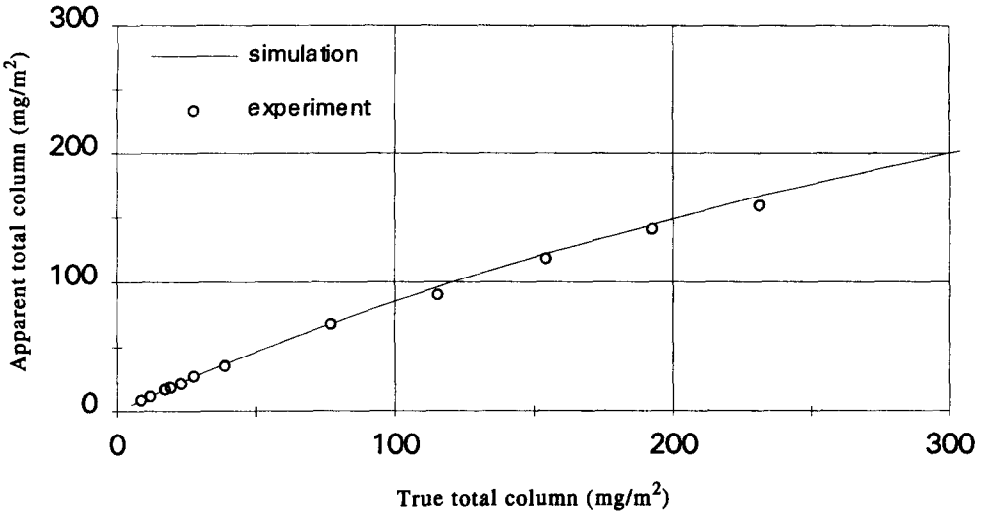

Fig. 10. Experimental and simulated apparent total columns of NO (obtained from DOAS evaluation) against the true total column.

the smaller magnitude (crosses) correspond to a total column of 176 mg/m^2, while the other spectrum (solid line) corresponds to a NO spectrum which has been simulated for a total column of 12.6 mg/m^2 and then been multiplied by a factor of 14, in order to correspond to a spectrum with a total column of 176 mg/m^2. The two spectra would be equal if the Beer–Lambert law were obeyed. It can be seen that the largest relative discrepancy between the spectra occurs at the absorption peaks and the main effect of nonlinearity on the absorption spectra is thus a reduction of the peak height. This is in agreement with the earlier conclusions drawn in Sec. 4.2.

Another observation to be made in Fig. 9 is that the shape of the residual is very similar to the shape of NO spectrum. This implies that when performing a spectral fit between the two spectra in the figure, most of the nonlinear effect will be observed as a quantitative decrease in the total column, rather than a qualitative decrease in the fit. This makes it difficult to discover nonlinearity effects from the quality of the spectral fit.

In Fig. 10 a comparison is shown between linearity curves for NO obtained from experimental recordings and from spectral simulations. The apparent total columns in experimental DOAS spectra were here retrieved by spectral fitting to a recorded calibration spectrum with a total column of 12.6 mg/m^2. The same procedure was also performed for the simulated spectra although a calibration spectrum corresponding to 12 μg/m^2 was used in this case. The simulated and experimental results agree within 5%. The simulation indicates that the NO absorption becomes nonlinear already at 6 mg/m^2 which corresponds to a peak OD of 0.024. This implies that also the used experimental calibration spectrum at 12.6 mg/m^2 is slightly nonlinear (approx. 2%). It should be noted that the nonlinearity limit is here defined as where the apparent OD deviates more than 1% from the true OD.

The influence of temperature and spectral resolution on the linear behavior of the NO spectra was also investigated by simulations. The results showed only minute differences, $<1\%$, in the linear behavior between 300 and 999 K and resolutions between 0.25 and 1 nm. The fact that the linearity curves seem independent of the spectral resolution agree with the discussion held regarding the hypothetical spectra in Fig. 5.

4.5. Nonlinearity of other species

Nonlinearity curves similar to the one for NO in Fig. 10 were also derived for the other species in this study. They were obtained by spectral fitting of recorded differential absorbance spectra at various total columns to calibration spectra, according to the procedure described in Sec. 3.1. In order to be able to compare several species in one figure, the apparent and true total columns were multiplied by the peak absorption cross-section for each species. This resulted in plots with apparent peak OD (as seen by the DOAS instrument) as a function of true peak OD for each species and this is shown in Fig. 11.

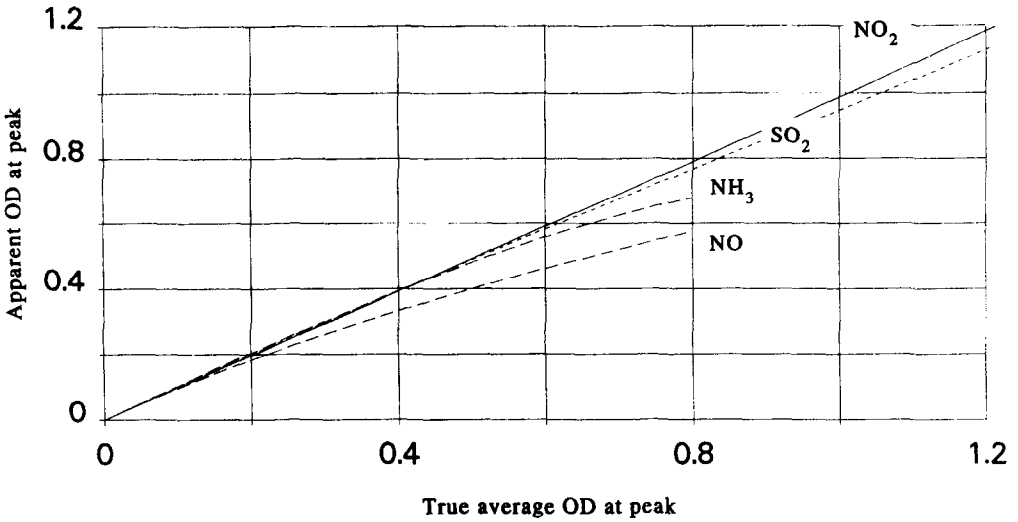

Fig. 11. Apparent optical depth at the maximum absorption peaks as a function of true average OD obtained from experimental recordings with the DOAS instrument used in this work.

Table 3. Region of linearity (< 1% deviation from linearity) for the differential absorption of several species (25°C, 1 bar).

Species	Region (nm)	Linear region (upper limit) mg/m²	OD†	A_1	A_2	A_3
NO	223–228	6	0.024	−1.663E-3	2.289E-6	−1.462E-9
SO_2	223–228	90	0.05	−1.235E-4	1.607E-7	−7.438E-10
SO_2	295–305	180	0.15	−5.875E-5	6.554E-9	
NH_3	212–217	36	0.35	1.1828E-3	−4.021E-5	−1.689E-9
NO_2	425–435	3150	0.7	6.3840E-6	−3.043E-9	

†Peak absorbance.

In analogy with Eq. (8), a polynomial with the coefficients A_1 to A_3 [Eq. (12)] can be fitted to the data shown in Fig. 11. In Table 3 a summary of the obtained coefficient is shown together with the obtained regions of linearity.

$$(c \cdot x)_{app} = (c \cdot x)_{true} + A_1 \cdot (c \cdot x)^2_{true} + A_2 \cdot (c \cdot x)^3_{true} + A_3 \cdot (c \cdot x)^4_{true}. \quad (12)$$

5. DISCUSSION

The results in this study give an interesting insight into how different gaseous species obey the Beer–Lambert law in the u.v./visible region. Three different types of absorption characteristics can be identified among the molecules studied, and these control to what degree the apparent absorption features follow the Beer–Lambert law.

NO exhibits the first type of characteristics where the true pressure-broadened absorption lines within the spectral bandpass of the instrument are many, 10–100, but mainly non-overlapping as was illustrated in Fig. 4. This means that the true OD will vary rapidly over the bandpass of the instrument yielding a large statistical variance of the spectrum. The apparent OD will therefore, according to Eq. (8) be equal to the true average OD only at very low optical depths. Since the difference between the true linewidths and the spectral bandpass is between one and two orders of magnitude a change in spectral resolution of the instrument will affect the spectral variance, and thereby the linear behavior, very little as was shown in the spectral simulations. This is also consistent with what was found from the calculations of the hypothetical spectra in Sec. 4.2. In the spectral simulations it was also found that the nonlinearity effect had only a very small temperature dependence for NO. According to Eq. (8) this implies that the variance of the absorption cross sections changes very little with the temperature.

The absorption of SO_2 between 200 and 230 nm also exhibits the same type of characteristics as NO around 226 nm, with considerable amount of fine structure in the spectra[20] and therefore a small linear region.

A second type of absorption characteristics is exhibited by the absorption of NO_2, for which the rotational lines are closer than for NO, and for which several electronic transitions overlap according to Takezava.[21] This creates continuous absorption spectra with little fine structure. Due to the continuous absorption structure the true averaged and the apparent ODs are equal up to large optical depths.

A third type of absorption characteristics can be seen for the absorption spectrum of ammonia. In the spectral region used for NH_3 measurements the molecule dissociates by predissociation,[22] and this is characterized by a sudden broadening of vibrational and rotational lines. This creates continuous spectra lacking rotational structure, although still exhibiting vibrational structure. The widths of the rotational absorption lines are several orders of magnitude larger than for NO,[23] and actually in the size range of the spectral bandpass of the DOAS instrument (0.2–0.5 nm). The linear region for the instrument will therefore be considerably larger than for NO. Since the linewidths are of the same order as the spectral bandpass, large effects in linear behavior will be seen when changing the resolution of the instrument, in agreement with the discussion in Sec. 4.3. When changing from a spectral bandpass of 0.24–0.16 nm the maximum linear OD for NH_3 changed from 0.4 to 1.15, for the absorption peak at 217 nm.

As was concluded above the nonlinearity effect mainly shows up as a quantitative change rather than a qualitative change in the spectral features. One way to extend the measurement region into the nonlinear region for various species, is therefore to compensate the retrieved concentrations after the spectral evaluation by a calibration curve, in the same manner as many extractive measurement instruments function today. This is discussed in an additional paper.[24]

Although the linearity was independent of temperature for NO this is not necessarily true for other species. Another interesting question is whether the nonlinearity is affected by spectral interference. In the spectral absorption region for NO there is interfering absorption from SO_2, and both species usually are present in flue gases.

Another interesting question is whether the nonlinearity effect is temperature dependent. The simulations for NO show only small changes in linear behavior between 300 and 1000 K even though the magnitude of the absorption cross sections change by at least 30%. This might not be the case for other species however.

In the study of nonlinearities the main systematic errors were uncertainties in the initial gas mixing ratios and these were in the order of 5%. The random errors were due to the mixing of the gas and these were below 1%. The absorption cross sections for NO could not be determined better than within 5% experimentally, due to the fact that NO is only linear at small total columns ($< 6\ mg/m^2$).

From the results in Fig. 11 it can be understood that large quantitative errors may be obtained when trying to detect species at large optical depths with the DOAS technique. In Table 4 typical flue gas concentrations are shown together with some performance data for the DOAS instrument in this study. The detection limits given were calculated with the assumption that the smallest detectable OD corresponded to 10^{-3} and spectral interferences were not included.

Table 4. Typical data for the DOAS instrument in this study and typical flue gas concentrations of various species. The optical pathlength of the DOAS is assumed to be 1 m. (All concentration values are given in mg/m^3.)

Species	Detection limit†	Linear region	Typical flue gas concentration	Typical relative errors
NO	0.25	6	1–1000	35% (at 300 mg/m^3)
NH_3	0.1	36	0.1–40	1.5% (at 40 mg/m^3)
SO_2 (226 nm)	1.4	90	1–2000	10% (at 2000 mg/m^3)
SO_2 (300 nm)	2	180	1–2000	5% (at 1000 mg/m^3)
NO_2	3.5	3150	0.1–100	0%

†Detection limits based on a smallest detectable OD of 10^{-3}, interference not included.

6. CONCLUSIONS

The main effect of the nonlinearity effect in the DOAS absorbance spectra is a change in peak height and it was found that most of the changes in the spectral features are quantitative rather than qualitative. By a simple mathematical derivation it was demonstrated that the deviations from linearity in the absorbance spectra are directly proportional to the variance of the true absorption cross sections, calculated over the bandpass of the instrument, and directly proportional to the square of the total column. This means that molecules with a large variation in the absorption cross sections over the bandpass of the instrument, e.g., NO, will be much more nonlinear than molecules with a smoother variation, e.g., NO_2 and SO_2. In cases where there are a large number of absorption lines within the bandpass of the instrument the nonlinearity effect will be fairly independent of the spectral resolution. This was shown by calculations of hypothetic spectra but also by simulations of the absorption spectrum of NO. The simulations also showed that the nonlinearity effect for NO was independent of temperature between 300 and 1000 K.

By arithmetic calculations it was found that the nonlinearity effect was most sensitive for changes in the instrument resolution when the absorption linewidths were in the same order of magnitude as the instrument, which is the case for NH_3 for instance. It was also shown that the resolution of the instrument has to be an order of magnitude smaller than the absorption linewidth in order to get a correct measurement of the true optical depth.

The total column regions, in which the relative deviations due to nonlinearity are less than 1% (linear region) are the following for the species studied: 6 mg/m^2 for NO, 90 mg/m^2 for SO_2 at 230 nm, 180 mg/m^2 for SO_2 at 300 nm, 36 mg/m^2 for NH_3 and 3150 mg/m^2 for NO_2. Some of these results, especially for NO contradicts what we have previously reported in preliminary results,[7] partly due to the fact that a more rigorous definition of the linear region was used. The results showed that relative errors as large as 35% can easily be obtained when performing DOAS measurements in a flue gas without compensating for the nonlinearity effect.

Acknowledgments—Financial support by the Thermal Engineering Research Association, Sweden (Project B7-010/020), and by the Nordic Industrial Fund (Project 90 1669) is gratefully acknowledged.

REFERENCES

1. D. Perner et al, *Geophys. Res. Lett.* **18,** 787 (1990).
2. S. Solomon et al, *J. Geophys. Res.* **92,** 8329 (1987).
3. G. W. Harris et al, Measurements of HONO, NO_3 and NO_2 by long-path differential absorption spectroscopy in the Los Angeles Basin, *Workshop on Optical and Laser Remote Sensing* 1982, Monterey, CA, 8–11 February, D3-1 (1982).
4. R. Gall, D. Perner, and A. Ladstätter-Weisenmayer, *Fresenius J. Analyt. Chem.* **340,** 646 (1991).
5. U. Platt and D. Perner, *Geophys. Res. Lett.* **7,** 89 (1980).
6. J. Mellqvist, H. Axelsson, and A. Rosén, *Analyst* **117,** 417 (1992).
7. J. Mellqvist, H. Axelsson, and A. Rosén, The DOAS technique in emission monitoring: temperature and nonlinearity effects, in *Incineration and Emission Control*, Berlin (June 1992).
8. A. Johansson, H. Axelsson, and J. Mellqvist, Continuous Monitoring of Ammonia by Differential Optical Absorption Spectroscopy (DOAS), in *Optical Sensing for Environmental Monitoring*, Atlanta (October 1993).
9. J. Mellqvist and A. Rosén, *JQSRT* **56,** 187 (1996).
10. H. J. Kostkowski and A. M. Bass, *JOSA* **46,** 1060 (1956).
11. R. J. Anderson and P. R. Griffiths, *Analyt. Chem.* **47,** 2339 (1975).
12. U. Platt and D. Perner, "Measurements of Atmospheric Trace Gases by Long Path Differential UV/Visible Absorption Spectroscopy", in *Optical and Laser Remote Sensing Techniques*, D. K. Killinger and A. Mooradian, eds., pp. 97–105, Springer, Heidelberg (1983).
13. P. R. Bevington, *Data Reduction and Error Analysis for the Physical Sciences*, McGraw-Hill, New York (1969).
14. M. Carleer, R. Colin, and A. C. Vandaele, *Technical Digest Ser.* **18,** 278 (1991).
15. T. Wahnström, A laser induced fluorescence study of OH radical desorption in the $H_2 + O_2$ reaction on Pt, dissertation, ISBN 91-7032-459-X, Chalmers University of Technology and University of Gothenburg, Gothenburg (1989).
16. K. P. Huber and G. Herzberg, *Constants of Diatomic Molecules*, Van Nostrand-Reinhold, New York (1979).
17. E. Hill and J. H. van Vleck, *Phys. Rev.* **32,** 250 (1928).

18. A. Y. Chang et al, *JQSRT* **47,** 375 (1992).
19. L. Råde and M. Rudemo, *Sannolikhetslära och Statistik för Teknisk Högskola*, Biblioteksförlaget, Stockholm (1984).
20. D. E. Freeman, K. Yoshino, J. R. Esmond, and W. H. Parkinson, *Planet. Space. Sci.* **32,** 1125 (1984).
21. S. Takezava, *Chem. Phys. Lett.* **97,** 77 (1983).
22. G. Herzberg, *Molecular Spectra and Molecular Structure III, Electronic Spectra and Electronic Structure of Polyatomic Molecules*, Van Nostrand-Reinhold, N.J. (1966).
23. L. D. Ziegler, *J. Chem. Phys.* **82,** 664 (1985).
24. J. Mellqvist, H. Axelsson, and A. Rosén, *JQSRT* **56,** 225 (1996).